electronics

MDPI

Article

Multi-Power Carriers-Based Integrated Control for Series-Cascaded Microgrid

Salman Ali [1], Santiago Bogarra Rodríguez [1,*], Muhammad Mansoor Khan [2] and Felipe Córcoles [1]

[1] Department of Electrical Engineering, Universitat Politècnica de Catalunya (UPC), 08222 Terrassa, Spain; salman.ali@upc.edu (S.A.); felipe.corcoles@upc.edu (F.C.)
[2] Key Laboratory of Control of Power Transmission and Conversion of Ministry of Education, Shanghai Jiao Tong University, Shanghai 200240, China; mansoor@sjtu.edu.cn
* Correspondence: santiago.bogarra@upc.edu

Abstract: Series-cascaded microgrids (SCMGs) indeed provide control flexibility and high-voltage synthesis capabilities. However, the power distribution in SCMGs based on distributed generation (DG) sources stays understudied. This paper proposes an SCMG topology using non-dispatchable DG sources and battery energy storage, with an integrated power-routing control. The objective is to address power distribution limitations and stabilize SCMG output voltages under varying conditions. A case study validates the control methodology, considering zero irradiation levels for photovoltaic (PV) and maximum power sharing. The battery modules play a crucial role by providing power, voltage support, and maintaining capacitor voltage at a reference value of a PV-integrated module. This is achieved through a third harmonic current injection in the fundamental frequency current, coupled with proportional power distribution using a third harmonic power signal. The effectiveness of the proposed SCMG topology and control is demonstrated through MATLAB/Simulink and hardware-in-loop analyses (Typhoon HIL). The results present an extended power distribution between series-cascaded DG sources-based units while ensuring stable SCMG output voltages, even in adverse conditions like PV module intermittency. Future work aims to extend the proposed topology to a ring/delta-connection SCMG, where third harmonic current aids power distribution among SCMG legs and between series-cascaded DG sources-based units.

Keywords: non-dispatchable; third harmonic current; integrated control; series-cascaded microgrid

Citation: Ali, S.; Rodríguez, S.B.; Khan, M.M.; Córcoles, F. Multi-Power Carriers-Based Integrated Control for Series-Cascaded Microgrid. *Electronics* **2024**, *13*, 446. https://doi.org/10.3390/electronics13020446

Academic Editor: Ahmed Abu-Siada

Received: 29 December 2023
Revised: 15 January 2024
Accepted: 19 January 2024
Published: 21 January 2024

1. Introduction

Microgrids (MGs) have gained popularity as a solution for coordinating and aggregating distributed generation (DG) sources, both in stand-alone and grid-integrated configurations. MGs can be categorized based on their configuration into two main types: paralleled and series-cascaded microgrids (SCMGs). While parallel MGs have undergone thorough research [1,2], their inherent requirement for parallel connected DG units to operate at the MG's rated voltage necessitates intermediate conversion stages with substantial input-to-output voltage boost ratios. This condition has the potential to escalate system costs and diminish overall MG efficiency. In this regard, one promising configuration is the SCMG, which allows for series-connected (SC) low-voltage DG sources to attain higher voltage levels and better utilization without the need for DC/DC boost converters in order to reduce cost while offering more control flexibility [3].

Initially designed for multilevel converters [4], cascaded converters have been subsequently extended for MG applications [5–8], named as SCMG [9]. In Figure 1a, each DG unit forms an MG system (MG*N*) with increased voltage levels through a series converter. Notably, the cascaded type has proven to be particularly practical in applications such as PV grid-connected systems [5] and battery management [6,10]. The SCMGs control methods can be applied to multilevel converter topologies, providing voltage and frequency support to the grid.

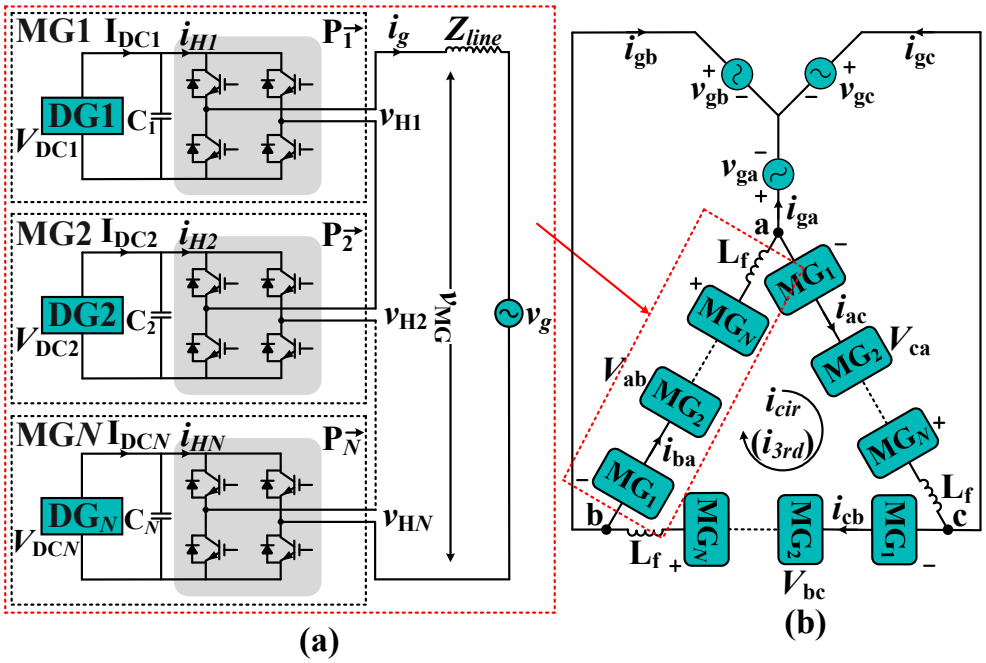

Figure 1. (**a**) DG-based series-cascaded microgrid topology. (**b**) Ring/delta connection of SCMGs.

Employing the DG modules of SCMG in grid-tied mode offers benefits, but synchronization and power-sharing issues can limit their application in MGs, affecting stability and AC-side support [7]. In the literature, the limitations of SCMG configurations using different DG sources-based modules have been discussed. One proposed solution utilizes a high-voltage DC link by connecting DC-DC converters with non-dispatchable DG sources (ND-DGs), and inverting the output using a DC-AC H-bridge [11]. Another topology cascades multiple H-bridges on an AC port to connect series-connected ND-DGs modules [12]. Maharjan et al. [6] studied an energy storage system in SC configuration. In [7], the focus was on dispatchable generation sources (D-DGs), ensuring a similar displacement power factor (*df*) among DG modules was vital for autonomous SCMG operation, achieved through inverse *df* droop control. However, this system is limited to inductive-resistive loads. Alternative control techniques, for instance, power factor angle control [13] and f-P/Q control [9] for D-DGs, achieved proportional power distribution and voltage synchronization for both resistive-capacitive and inductive loads. Hierarchical control approaches [14] maintain frequency and voltage regulation in SC energy storage and SCMG systems. A distributed control methodology that uses inverse droop at the local controller and standard droop at the central controller to manage power for SCMG energy storage systems in both grid-connected and islanded modes was developed in [15]. Distributed control systems based on communication enable power sharing among cascaded ND-DGs modules [16]. Li et al. [17] proposed a communication-dependent SC voltage and current-controlled MG for grid-tied operation. Decentralized control methods [18–21] considered D-DGs modules for power sharing.

Complex control strategies are essential for SCMG systems to attain performance goals such as grid synchronization, AC output voltage regulation, maximum point tracking (MPPT), power sharing, and grid voltage support, regardless of the topology used in [19]. The cascaded DG-based modules pose challenges due to shared current. The D-DGs offer complete controllability and stable voltage, as presented in [22], while ND-DGs that operate with limited load current require centralized control strategies. The power sharing among multiple DG sources-based modules connected in series is a primary concern in SCMGs and especially with various combinations of DG sources-based modules. In the literature, the SCMG structure is based on different combinations of D-DGs and ND-DGs modules; meanwhile, some configurations integrated with energy storage systems working as smoothers

in series/parallel to DG modules have been analyzed [7,9,11–19,21,23–25]. The existing literature on SCMGs lacks adequate exploration of power distribution dynamics between cascaded ND-DGs (PV) and energy storage systems. Particularly, the involvement of battery modules in extended power-sharing to tackle intermittent PV generation remains under-addressed, especially during worst-case scenarios. Despite SCMGs' presence, previous studies have explored different power-sharing techniques for CHB-based PV systems to mitigate uneven power distribution.

Power-routing control methods in cascaded PV systems utilize fundamental voltage reconstruction as developed in [12,24–26], and third harmonic voltage injection is presented in [27,28]. Although fundamental voltage reconstruction distributes the active component of each DG-based module's output voltage proportionally to its DC-side input power, it has a limited power distribution range. To overcome this limitation, third harmonic voltage injection was introduced, improving DC voltage utilization by increasing modulation. However, this method primarily focuses on phase-leg balancing and does not account for unbalanced phase-leg voltages due to module failures or intermittent renewables. In the literature, centralized and decentralized power distribution techniques are discussed for a limited power-sharing range in grid-connected SCMGs.

Considering the constraints mentioned earlier in SCMGs, such as the practical combinations of DG-based modules and power-sharing limitations arising from the intermittent nature of ND-DGs [29–31], this paper introduces a multi-power carriers-based integrated power distribution control approach. The aim is to overcome power-sharing limitations and provide voltage support in SCMGs featuring ND-DGs and storage systems. To attain an extended power-sharing range, a third harmonic current is injected into the fundamental frequency current. In an SCMG structure (Figure 1a), this third harmonic current appears in the grid current. However, in the extended ring/delta connection of SMGs, the third harmonic current will circulate within the system (i_{cir}(i_{3rd})) rather than flowing towards the grid (Figure 1b). The injected third harmonic current will perform power-sharing with the PV integrated module from the battery based over a third harmonic power while stabilizing its capacitor voltage to the reference value. This, combined with proportional power distribution between the modules, means that the power-sharing control range is significantly increased while maintaining the output voltages of the cascaded DG sources-based modules. A case study is conducted to validate this through MATLAB/Simulink and Typhoon HIL, considering a maximum power distribution range and zero PV irradiation. Battery modules ensure grid stability and provide necessary power and voltage support in absence of PV power generation.

Section 2 introduces the generic SCMG schematic and the specific SCMG topology studied in this paper, along with their operating principles. In Section 3, a comprehensive analysis of the proposed multi-power carriers-based integrated control methodology is provided. The validity of the proposed SCMG and its control methodology are examined through simulation and emulation in Section 4. Finally, the future work is outlined in Section 5, and the conclusions are summarized in Section 6.

2. DG-Based Series-Cascaded Microgrid

The schematic of the DG sources-based SCMG is depicted in Figure 1a. Unlike the conventional two-stage DG-based module interface, the DG source is in direct connection to the DC/AC LV interfacing converter. This generates a lower output AC voltage for each module, which is not in a suitable range for MG integration. However, combining SCMGs' AC output voltages provides essential frequency and voltage support to the grid.

The SCMG consists of N series-connected DG-based modules (MGN), where each module constitutes an H-bridge and a DG source on the DC-side. The i_g and v_g are grid current and voltage, respectively; $\mathrm{I_{DC}}_i$ and $V_{\mathrm{DC}i}$ are the DC-link current and voltage of

*i*th (i = 1, 2, …, N) module, respectively; $v_{\mathrm{H}i}$ is the output voltage of the *i*th module. In grid-connected mode, the active and reactive power of the *i*th DG source-based module are:

$$P_i = \mathrm{Re}\left(v_i e^{j\delta_i} \left(\frac{v_{\mathrm{MG}} e^{j\delta_{\mathrm{MG}}} - v_g e^{j\delta_g}}{|Z_{line}| e^{j\theta_{line}}} \right)^* \right) \tag{1}$$

$$Q_i = \mathrm{Im}\left(v_i e^{j\delta_i} \left(\frac{v_{\mathrm{MG}} e^{j\delta_{\mathrm{MG}}} - v_g e^{j\delta_g}}{|Z_{line}| e^{j\theta_{line}}} \right)^* \right) \tag{2}$$

where δ_g is the grid phase angle. v_i and δ_i are the voltage amplitude and phase angle of the *i*th DG-based module, respectively. v_{MG} and δ_{MG} are the voltage amplitude and phase angle at point of common coupling between MGN and the utility grid, respectively. θ_{line} is the circuit's impedance angle. For a medium/high voltage network, the line impedance is mainly inductive. The voltage at point of common coupling v_{MG} is as follows:

$$v_{\mathrm{MG}} e^{j\delta_{\mathrm{MG}}} = \sum_{i=1}^{N} v_{\mathrm{H}i} e^{j\delta_{\mathrm{H}i}} \tag{3}$$

Hence, the power transfer attributes of the *i*th MG unit are as follows:

$$P_i = \frac{v_i}{|Z_{line}|} \left(v_g \sin(\delta_i - \delta_g) - \sum_{j=1}^{N} v_j \sin(\delta_i - \delta_j) \right) \tag{4}$$

$$Q_i = \frac{v_i}{|Z_{line}|} \left(\sum_{j=1}^{N} v_j \cos(\delta_i - \delta_j) - v_g \cos(\delta_i - \delta_g) \right) \tag{5}$$

As per Figure 1a, the dynamic characteristics of SCMG are as follows:

$$\frac{di_g}{dt} = \frac{1}{\mathrm{L}} \left(\sum_{i=1}^{N} V_{\mathrm{HF}i} - R i_g - v_g \right) \tag{6}$$

According to phasor theory and by ignoring the equivalent resistance R, we obtain the following:

$$\sum_{i=1}^{N} V_{\mathrm{HF}i} = \sum_{i=1}^{N} k_i V_{\mathrm{DC}i} = V_g + j\omega \mathrm{L} I_g \tag{7}$$

where ω is the grids' angular frequency; $V_{\mathrm{HF}i}$ is the phasor form of $v_{\mathrm{HF}i}$ (fundamental component); k_i represents the control signal of each module; and V_g and I_g are the phasor forms of v_g and i_g, respectively. The SCMGs' equivalent AC circuit is shown in Figure 2a and the phasor diagram in Figure 2b, where the voltage component of inductance L is significantly smaller compared to the grid voltage, allowing for δ to approximate zero.

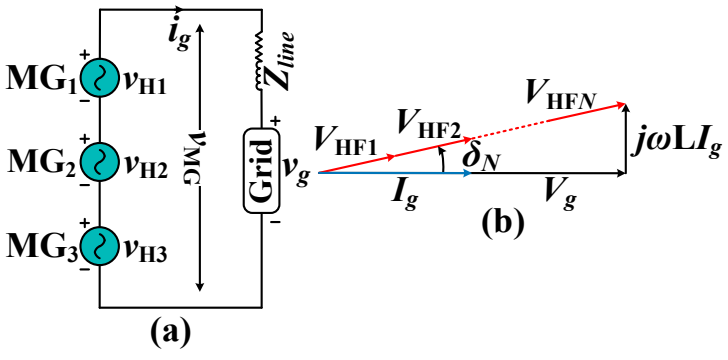

Figure 2. (**a**) Equivalent AC circuit of DG-based SCMGs, (**b**) Phasor diagram of grid-connected DG-based SCMGs.

The current of all series MG*N* units (Figure 2a) is inherently equal and cannot be varied individually. Thus, the operating voltage of each MG unit must be in direct relation to its power rating to ensure proportional power-sharing between them.

$$v_{o\_i} \propto P_{\max\_i} \tag{8}$$

where v_{o_i} is a reference or nominal operating voltage of ith unit and $P_{\max\_i}$ is the rated or maximum power of ith unit. While the nominal operating voltage of each MG is set based on (8), the sum voltages of SCMGs must be equal to user-level voltage.

$$v_{o\_1} + v_{o\_2} + \ldots + v_{o\_N} = v_{\mathrm{MG}} \tag{9}$$

At maximum load operating condition, Equation (9) becomes:

$$v_{o\_1} i_{max\_1} + v_{o\_2} i_{max\_2} + \ldots + v_{o\_N} i_{max\_N} = v_{\mathrm{MG}} i_{max\_\mathrm{MG}} \tag{10}$$

$$P_{max\_1} + P_{max\_2} + \ldots + P_{max\_N} = P_{T\_AC} \tag{11}$$

where P_{T_AC} is the total active rated power output of SCMG. As power is fed to a relatively stable voltage grid, the power control can be achieved indirectly by regulating output current i_g using Equation (1) and Figure 2a,b. If the power factor will be 1, the output reference current could be as follows:

$$i'_{g\_ref} = \frac{P_{\mathrm{T}}}{v_g \sin(\delta_i - \delta_g)} \tag{12}$$

2.1. Proposed Non-Dispatchable DGs and Energy Storage-based Series-Cascaded Microgrid

The proposed SCMG includes MG1 with PV followed by a set of battery-based modules. The MG2 and MG3 will serve as stabilizers, supplying necessary grid support via power distribution control. This accounts for varying operating conditions resulting from intermittent PV behavior. However, due to the power distribution control limitations mentioned in Section 1, the battery modules can only deliver a proportion of power, of which a solution is proposed in Section 3.

2.2. Operating Principle

In the unipolar PWM-based 7-level SCMG, the output voltage is a sum of 3-level module voltages (Equation (9)). From Equations (9)–(11), the proposed SCMG structure can present the following operations:

1. $P_{PV} > P_{AC}$, $(P_{PV} \rightarrow |P_{AC}| + |P_B|)$, batteries charging, Figure 3a.
2. P_{AC} disconnected, $(P_{PV} \rightarrow |P_B|)$, batteries charging, Figure 3b.
3. $P_B = 0$, $(P_{PV} \rightarrow |P_{AC}|)$, PV supplying power to grid, Figure 3c.
4. $P_{PV} = 0$, $(|P_{AC}| \rightarrow |P_B|)$, batteries charging, Figure 3d.
5. $P_{PV} < P_{AC}$, $(P_{PV} + P_B \rightarrow |P_{AC}|)$, batteries discharging, Figure 3e.
6. $P_{PV} = 0$, $(P_B \rightarrow |P_{AC}|)$, batteries discharging, Figure 3f.

In the SCMG literature, solutions are presented for low/high PV irradiation levels. However, no solution is provided for operating condition 6, where PV panels are unable to supply grid power while preserving module output AC voltage levels ($2N + 1$) and system stability. To address this, a solution is shown in Figure 4, introducing a multi-power carriers-based integrated power-routing control. This approach extends the power-sharing range and includes third harmonic power-dependent proportional power-sharing, detailed in the next section.

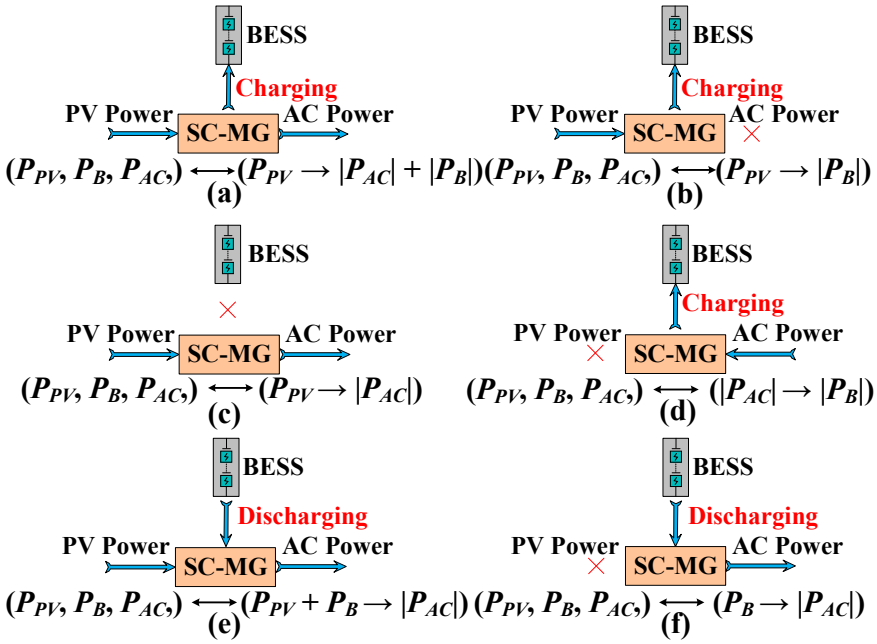

Figure 3. (**a**–**f**) SCMG operation modes and corresponding power flow.

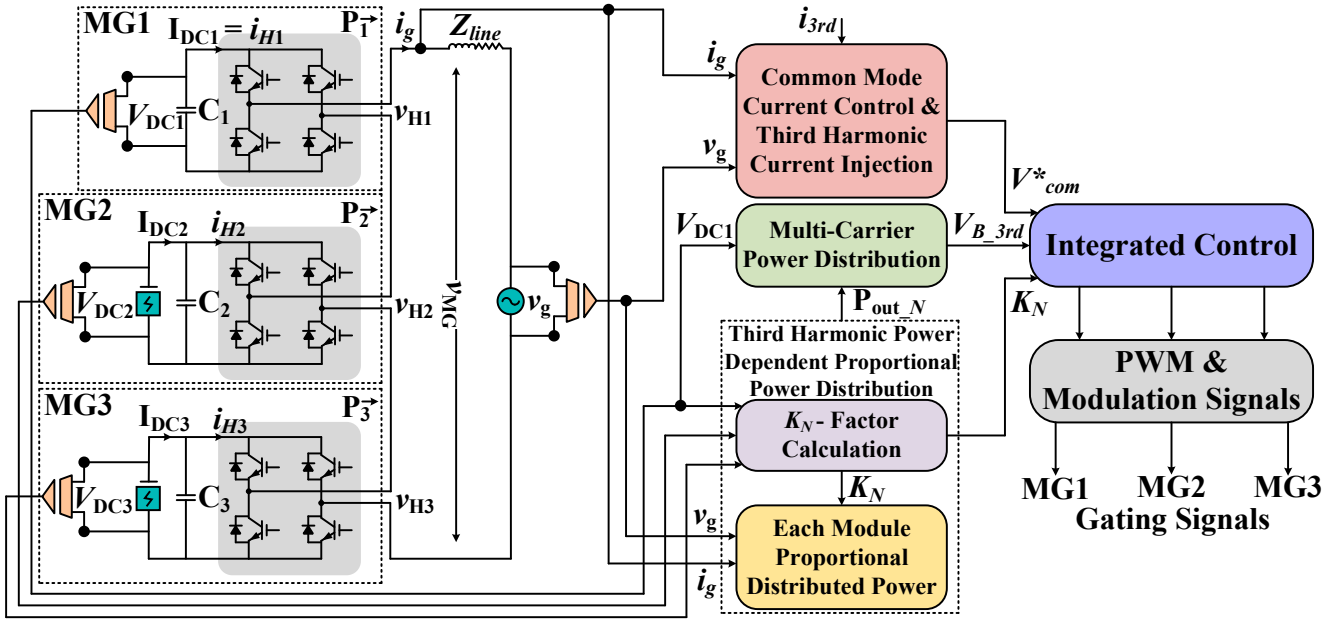

Figure 4. SCMG based on ND-DGs (PV = 0) and battery energy storage system.

3. Proposed Multi-Power Carriers-Based Integrated Control Methodology

The integrated control methodology consists of multiple components, including a current control loop based on third harmonic current injection and a multi-power carriers-based power distribution loop between DG sources- modules. Notably, the fundamental principle extends seamlessly to a higher number of DG sources-based SC modules, continually enhancing the power-sharing capabilities among the cascaded units. The role of a current control loop is to ensure the regulation of grid current. The power distribution control enhances the power-sharing range while reducing the number of voltage control loops by implementing a third harmonic power-dependent proportional power-sharing mechanism between SC-DG sources-based modules. The control structure of the SCMG is presented in Figure 4 and the block diagram of DG-units-based SCMG is shown in Figure 5.

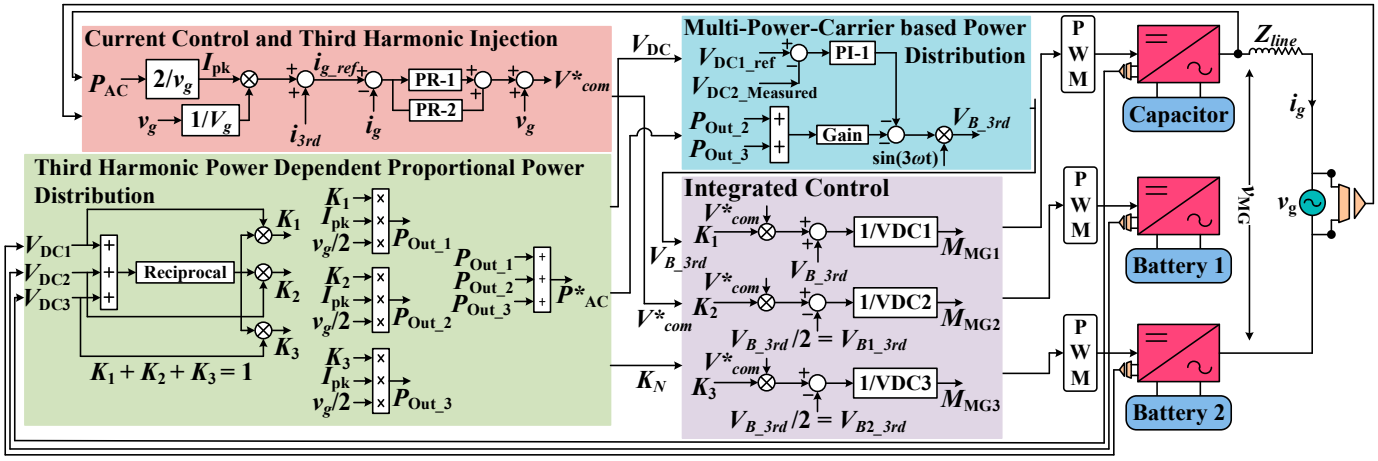

Figure 5. Multi-carrier-based integrated control for optimized power distribution.

3.1. Third Harmonic Current-Injected Current Control Loop

Examining Figure 4 and Equation (11) reveals the total power's reliance on the sum of cascaded modules' powers. Nevertheless, an unbalanced active power in DG modules arises if control solely centers on the fundamental frequency current. This occurs because MG1, which is solely capacitor-integrated, lacks a generation source, hindering active power delivery. Thus, to attain power distribution across MG*N* units and enable total active power transfer, the third harmonic current is devoted to being a power carrier. So, the fundamental frequency current can be calculated from Equation (13).

$$P_{T\_AC} = \frac{1}{2} V_M I_M \tag{13}$$

where V_M and I_M are v_g and i_g amplitudes, respectively. Before delving into the third harmonic current-injection approach, grasping common- and differential-mode quantities is essential. In series-cascaded configurations, the common-mode power embodies the shared power among modules, representing the collective average power that the fundamental frequency current regulates, subsequently channeling to the grid. In contrast, the differential-mode power denotes the power variance between adjacent series-cascaded modules. This component is module specific, dedicated by voltage disparities. The differential-mode power serves as the conduit for power or information exchange across modules. Managing the differential-mode power is pivotal for realizing targeted module power distribution, overall system stability, and efficiency preservation. This understanding underpins the efficacy of the subsequent third harmonic current-injection methodology. With this understanding, the SCMG structure injects the third harmonic current into the fundamental frequency current. This serves as a power carrier, enabling efficient control and distribution of differential-mode power across SCMG-DGs while offering grid voltage support. Following this injection, the fundamental line current flowing through the series-cascaded DG units can be:

$$i_{line} = i_{\mathrm{F}} \sin(\omega t + \theta_v + \varphi_1) + i_{3rd} \sin(3\omega t + 3\theta_v + \varphi_3) \tag{14}$$

where i_{F} and φ_1 are the amplitude and angle of fundamental line current, respectively. Here, ω is the line frequency and θ_v assumes the phase angle. i_{3rd} and φ_3 are the amplitude and angle of the third harmonic current, respectively. Moreover, the injection of third harmonic current will induce the third harmonic voltage in a cluster voltage (v_{cl}).

$$v_{cl} = v_{\mathrm{F}} \sin(\omega t + \theta_v + \delta_1) + v_{3rd} \sin(3\omega t + 3\theta_v + \delta_3) \tag{15}$$

To manage differential-mode power via third harmonic current injection, it is noted that if the sum of third harmonic voltages in-phase with the third harmonic current is

zero, it facilitates module-to-module power exchange without altering the third harmonic current or affecting grid power exchange.

Precise control of the third harmonic current amplitude is essential to achieving equilibrium between the grid current peak amplitude and the AC-side voltage delivery limit of each DG unit. Analyzing third harmonic current amplitude necessitates recognizing that, in SCMGs for proportional power-sharing, the module's active power (P_{AC_N}) is a function of its AC voltage V_{AC_N} and current i_{AC}. Additionally, each module's active power output aligns with its DC power. Hence, a proportional power-sharing factor (k_N) is defined as a ratio of desired module active power output to total the active power output (P_{T_AC}) of SCMG:

$$P_{AC\_N} = k_N \times P_{T\_AC} \tag{16}$$

Each module's maximum AC-side voltage delivery limit, studied by its available DC voltage, is denoted as $V_{ACMax\_N|V_F+V_{3rd}|}$. This limit encompasses fundamental (V_F) and third harmonic voltage components (V_{3rd}), determined via relation:

$$V_{ACMax\_N|V_F+V_{3rd}|} \leq V_{DC\_N} \tag{17}$$

Here, V_{DC_N} signifies the DC-side voltage of each module. Equation (17) highlights that the total DC-side voltage (V_{T_DC}) should be equal to or exceed the sum of maximum AC-side voltage delivery limits, incorporating in-phase and quadrature control voltage components denoted as V_{CN}. The relation is as follows:

$$V_{T\_DC} \geq \sum_{N=1}^{3} V_{ACMax\_N|V_F+V_{3rd}|} + V_{CN} \tag{18}$$

Initially, common-mode and differential-mode power distributions adjust via fundamental voltage manipulation. However, if residual differential power remains, third harmonic current is introduced for its transfer. The key objective is to inject an optimal third harmonic current within the system limits specified in Equation (18). As power distribution hinges on the third harmonic current, adherence to maximum system current limit is vital. This peak limit, based on the RMS value, designates third harmonic current as i_{3rd_RMS}, maximum MG current limit (RMS) as i_{AC_RMS}, and fundamental frequency current as i_{F_RMS}.

$$i_{3rd\_\mathrm{RMS}} + i_{F\_\mathrm{RMS}} \leq i_{AC\_\mathrm{RMS}} \tag{19}$$

Furthermore, active power distribution relies on a chosen output voltage amplitude, given the shared current in each DG unit. While SCMG module voltage magnitudes differ from MG's rated voltage, voltage phase synchronization among modules is crucial for effective power sharing. Third harmonic current inclusion aids this voltage phase alignment within series-cascaded modules. Thus, to optimize operation, each DG unit's active power encompasses fundamental and third harmonic current. The module's maximum power, constrained by maximum output power, is defined as;

$$P_{ACMax\_N|V_F+V_{3rd}|} = \frac{P_{ACNom\_N|V_F+V_{3rd}|}}{P_{T\_ACNom}} P_{T\_AC} \tag{20}$$

where $P_{ACMax\_N|V_F+V_{3rd}|}$ is the maximum AC-side power of each module, $P_{ACNom\_N|V_F+V_{3rd}|}$ is the nominal AC-side power of each module, and P_{T_ACNom} is the nominal output power of SCMG. However, all the series-cascaded units share the same current; so, Equation (20) can be described to obtain the maximum AC-side voltage of each module:

$$V_{ACMax\_N|V_F+V_{3rd}|} = \frac{V_{ACNom\_N|V_F+V_{3rd}|}}{V_{T\_ACNom}} V_{T\_AC} \tag{21}$$

By considering the system parameter limitations as defined in Equations (18)–(21), the amplitude of the third harmonic current could be adjusted. If the amplitude of i_{3rd}

would be much higher, then it would exceed the constraint defined in Equation (17), which means that a larger proportion of the grid current is allocated to third harmonic component. Conversely, the decrease in the amplitude of i_{3rd} would exceed the AC-side voltage delivery limit. Hence, the amplitude of third harmonic current can be controlled to achieve power distribution while considering maximum voltage limits and current constraints in the SCMG structure. Considering these conditions, the third harmonic current-injection constraints could be defined as:

$$\begin{cases} i_{AC\_Max} - i_F \geq i_{3rd} \\ V_{ACMax\_1}|V_{F\_1}+V_{3rd\_1}| \leq V_{AC\_1} \\ V_{ACMax\_2}|V_{F\_2}+V_{3rd\_2}| \leq V_{AC\_2} \\ V_{ACMax\_3}|V_{F\_3}+V_{3rd\_3}| \leq V_{AC\_3} \end{cases} \text{where } i_{3rd} > 0 \quad (22)$$

Comparing grid reference current i_{g_ref}, with grid current i_g, two PR controllers govern the process. The PR-1 is tuned at fundamental frequency, while PR-2 is tuned at three times the fundamental frequency, regulating third harmonic current. PR controllers are preferred over PI controllers as they can track sinusoidal references without steady-state errors. The output control command of current loop is then multiplied by each module's k_N-factor within an integrated loop, as determined by DC-side voltage. It eases third harmonic power based proportional power-sharing between cascaded modules. The estimation process for k_N-factor is elaborated in subsequent sub-section.

3.2. Determining k_N-Factor for Third Harmonic Power-Dependent Proportional Power Distribution

Fundamental proportional power sharing is an existing technique, addressing power distribution among cascaded modules with limited power-routing range. It allocates the active component of each module's output voltage in line with its DC-side input power. To enhance the power-sharing range, this paper employs third harmonic power for proportional sharing between series-cascaded modules. To attain this power distribution, this section calculates each module's active power capability relative to fundamental power capacity by first determining the k_N-factor. For every module (N = 1, 2, 3), k_N-factor equates its DC-side power to total DC-side power, ensuring AC-side active power output's proportionality to DC-side power.

$$k_N = \frac{P_{DCN}}{P_{DC\_Total}} \quad (23)$$

The k_N-factor is then multiplied by total active power output P_{T_AC} to determine the fundamental proportional power of Nth module relative to its power capacity and total active output power. It is important to ensure that sum of all k_N-factors is equal to 1, indicating a balanced power distribution.

$$k_1 + k_2 + \ldots + k_N = 1 \quad (24)$$

Considering the above condition, the k_N-factor is utilized for fundamental power distribution between modules, where each module's active power ratio is proportional to its DC-side power. After fundamental proportional power-sharing, the remaining power is compensated through third harmonic power, which can be determined by subtracting the fundamental power P_{F_N} from active power output of each module.

$$P_{3rd\_N} = P_{AC\_N} - P_{F\_N} \quad (25)$$

As the k_N-factor is introduced in Equation (16), for the proportional power-sharing of each module, the fundamental power-sharing of each module can be defined via fundamental ratio:

$$P_{F\_N} = \beta P_{AC\_N} \quad (26)$$

In the above equation, the β is a proportional power-sharing factor for the fundamental frequency. By utilizing Equations (25) and (26), the function for the remaining third harmonic power-sharing capability of each module can be realized:

$$P_{3rd\_N} = (1 - \beta)P_{AC\_N} \tag{27}$$

Due to the series connection of modules and series current flow, the third harmonic power-sharing capability of each module defined in Equation (27) can be represented in voltages in Equation (28); here, according to Equations (16), (17) and (23), the AC-side active power of each module is linked with the DC-side voltage of a specific module. So, if the factor 1-β is positive in Equation (27), the module could have the capability to share power with other modules and vice versa.

$$V_{3rd\_N} = (1 - \beta)V_{DC\_N} \tag{28}$$

The calculated proportional distributed power through k_N-factor for each module is integrated with the multi-power carriers-based power distribution methodology, which is explained in the subsequent sub-section.

3.3. Multi-Power Carriers-Based Power Distribution

To enhance DC-side voltage utilization during power exchange in modules, power distribution involves adjusting the reference for each module. In series clusters with varying module powers, the average DC-link voltage remains constant, but individual module voltages differ. Traditional control methods lack the ability to implement power distribution via third harmonic current injection in fundamental frequency current. In the proposed multi-power carrier-based power distribution methodology, the third harmonic current is considered a carrier for power distribution among the modules. The third harmonic current is the component of circulating current in the ring/delta structure (Figure 1b), which does not appear in the grid current and voltage. However, in a series-cascaded system, it will appear in the output voltage and current as mentioned in the mathematical analysis in previous sections. Moreover, due to the injection of the third harmonic current in the fundamental frequency current, the output power of each module constitutes the fundamental and third harmonic power. However, due to the proposed integrated control approach, the total third harmonic power of all the modules would be zero.

The principle of multi-carrier-based power distribution control is to deliver the required power support from the battery modules to PV-based modules through third harmonic power distribution. To achieve power distribution among modules, the total third harmonic power is regulated by controlling the actual DC-link voltage V_{DC1} of MG1 to match the reference value, along with the power shared from battery modules. Stabilizing V_{DC1} at the reference value involves comparing it with $V_{\mathrm{DC1\_}ref}$ to generate an error signal fed into a PI controller, minimizing the deviation between actual and reference capacitor voltages. The PI controllers' output is added to the required third harmonic power from MG1, induced through battery modules. This creates a third harmonic signal that, when multiplied, allows for the total third harmonic power distribution signal to resonate at the third harmonic frequency, shown in Figure 5.

The optimal proportional power for power distribution of each series-cascaded DG-based module can be obtained from Equation (19). Due to the addition of a third harmonic component, the total power of N modules can be represented as:

$$P_{N\_total} = P_{\mathrm{F\_}total} + P_{3rd\_total} = \sum_{i=1}^{N} P_{\mathrm{F\_}N} + \sum_{i=1}^{N} P_{3rd\_N} \tag{29}$$

Based on Equations (14), (15) and (29), the total average power of N modules can be represented as:

$$P_{N\_avg} = \frac{1}{\mathrm{T}} \int_0^{\mathrm{T}} (P_{\mathrm{F}\_total} + P_{3rd\_total}) dt \tag{30}$$

So, according to Equations (14) and (15), Equation (30) can become the following:

$$P_{N\_avg} = \frac{1}{\mathrm{T}} \int_0^{\mathrm{T}} \left[\begin{array}{l} \{v_{\mathrm{F}} \sin(\omega t + \delta_{1\_\mathrm{F}}) i_{\mathrm{F}} \sin(\omega t + \varphi_{1\_\mathrm{F}})\} + \\ \{v_{3rd} \sin(3\omega t + \delta_3) i_{3rd} \sin(3\omega t + \varphi_3)\} \end{array} \right] dt \tag{31}$$

Referring to trigonometric identities, Equation (31) becomes the following:

$$P_{N\_avg} = \frac{1}{\mathrm{T}} \left[\begin{array}{l} \frac{v_{\mathrm{F}} i_{\mathrm{F}}}{2} \int_0^{\mathrm{T}} \{\cos(\delta_{1\_\mathrm{F}} - \varphi_{1\_\mathrm{F}}) - \cos(2\omega t + \delta_{1\_\mathrm{F}} + \varphi_{1\_\mathrm{F}})\} dt \\ + \frac{v_{3rd} i_{3rd}}{2} \int_0^{\mathrm{T}} \{\cos(\delta_3 - \varphi_3) - \cos(6\omega t + \delta_3 + \varphi_3)\} dt \end{array} \right] \tag{32}$$

So, by solving the above equation, the instantaneous power of N modules can be obtained:

$$\begin{array}{l} P_{N\_inst} = \frac{v_{\mathrm{F}} i_{\mathrm{F}}}{2\mathrm{T}} \left[\mathrm{T} \cos(\delta_{1\_\mathrm{F}} - \varphi_{1\_\mathrm{F}}) - \frac{1}{2\omega} \left\{ \begin{array}{l} \sin(2\omega \mathrm{T} + \delta_{1\_\mathrm{F}} + \varphi_{1\_\mathrm{F}}) \\ -\sin(\delta_{1\_\mathrm{F}} + \varphi_{1\_\mathrm{F}}) \end{array} \right\} \right] \\ + \frac{v_{3rd} i_{3rd}}{2\mathrm{T}} \left[\mathrm{T} \cos(\delta_3 - \varphi_3) - \frac{1}{6\omega} \left\{ \sin(6\omega \mathrm{T} + \delta_3 + \varphi_3) - \sin(\delta_3 + \varphi_3) \right\} \right] \end{array} \tag{33}$$

After this, the total third harmonic voltage V_B_3rd is applied to the integrated control where it is superimposed on the duty cycle signal V^*_{com} to form the final duty cycle signal of a module for unipolar phase-shifted PWM. The superimposition of V_B_3rd for integrated control is explained in the next sub-section.

3.4. Integrated Control Approach

The integrated control approach offers the capability to superimpose the V_B_3rd for power distribution among the modules. The advantage of this superimposition is that it makes the sum of the third harmonic power distribution between the modules equivalent to zero.

$$P_{3rd\_1} + P_{3rd\_2} + \ldots + P_{3rd\_N} = 0 \tag{34}$$

According to the condition described in Equation (34), the sum of third harmonic power distribution between the modules must be equivalent to zero. However, the direction of the third harmonic current in all the modules is the same. Hence, the sum of third harmonic voltages must be equivalent to zero, eventually leading to the zero sum of third harmonic power.

The detailed phasor diagram for fundamental and third harmonic components is illustrated in Figure 6. The fundamental cluster voltage (v_{F}) and the third harmonic cluster voltage amplitudes (v_{3rd}) are depicted. In SCMG, when the first module has PV Power, it could be assumed that all three modules operate at equilibrium. However, if the first module experiences a disturbance, the power-sharing ratio of the other two modules may change to overcome this issue. Therefore, the third harmonic current injection enables effective differential-mode power control, extending the power-sharing range. Orienting the grid voltage vector v_g as the d-axis, and the perpendicular direction as the q-axis, v_{F_N} is the fundamental voltage vector of the Nth module; V_F is the vector of the fundamental voltage output by inverter; v_{F_Nd} and v_{F_Nq} are the voltage vectors of v_{F} on the d-axis and q-axis, respectively. Here, the angle δ representing the third harmonic components angle is three-times the angle θ representing the fundamental components angle. The phasor diagram reveals that the total third harmonic voltages required by the PV module

are superimposed in the duty cycle signal of MG1 and half of the total third harmonic voltages are subtracted from MG2 and MG3. The resultant third harmonic vector (v_R_3rd) is represented in Figure 6b. As the modules distribute active power, the q-component of the third harmonic resultant vector approaches zero, allowing the power exchange between modules utilizing differential-mode power.

$$v_{R\_3rd\_d}\cos\delta = \sum_{N=1}^{3} v_{3rd\_Nd}\cos\delta_N = v_{3rd\_1d}\cos\delta_1 + v_{3rd\_2d}\cos\delta_2 + \ldots + v_{3rd\_Nd}\cos\delta_n \quad (35)$$

$$v_{R\_3rd\_q}\sin\delta = \sum_{N=1}^{3} v_{3rd\_Nq}\sin\delta_N = v_{3rd\_1q}\sin\delta_1 + v_{3rd\_2q}\sin\delta_2 + \ldots + v_{3rd\_Nq}\sin\delta_N \quad (36)$$

The third harmonic resultant vector's d and q components are defined, so the overall expression of resultant vector is as follows:

$$v_{3rd\_1} + v_{3rd\_2} + \ldots + v_{3rd\_N} = \sum_{N=1}^{3} v_{3rd\_N} = v_{R\_3rd} \quad (37)$$

It is clear that to control differential-mode power for power sharing, the sum of third harmonic voltages in-phase with third harmonic current should be zero, which will lead to a zero sum of third harmonic power while satisfying the condition in Equation (34).

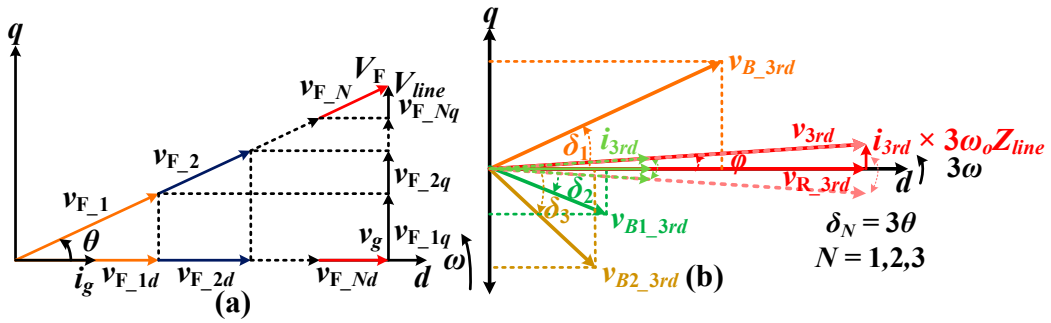

Figure 6. Phasor diagram of SCMG: (**a**) fundamental components; (**b**) third harmonic components.

4. Validation and Results

To verify the effectiveness and performance of the proposed SCMG structure depending on multi-power carriers-based integrated optimal power distribution control, simulations were carried out on MATLAB/Simulink platform. The simulation model is comprised of three MGs in a series-cascaded connection (Figure 3). The related simulation parameters are listed in Table 1. As mentioned above, the case for operating condition 6 in Figure 4 is considered for the performance analysis of the developed control methodology. Further, to examine the power-sharing range of the developed control in order to maintain the seven-level output voltages, a simulation is carried out for three different cases.

Case #1: Power distribution when $V_{B1} + V_{B2} > v_{g\_pk}$

The SCMG system was implemented in this scenario with V_{DC2} = 165 V for the battery module voltage in MG2 and V_{DC3} = 165 V for the battery module voltage in MG3, where the batteries are in a discharging state in all the cases. The DC-side rated voltage was set to 405 V for all the cases by stabilizing the MG1 capacitor voltage to a reference value. Therefore, in this case, the capacitor voltage in MG1 needed to be balanced at V_{DC1} = 75 V through multi-power-carriers-based power distribution while ensuring that the SCMG output step-voltages were maintained at v_{MG} = 405 V.

Figure 7a indicates that the output step-voltages remained stable over time during MG1's capacitor voltage balancing, with stable grid current and in-phase with the grid voltage. The injected third harmonic current is present in the grid current (Figure 7a) as it

should appear in the single phase according to the control methodology (Figure 5). The significance of the third harmonic current injection in fundamental frequency current can be seen in Figure 7b, where it balanced MG1 capacitor voltages at the reference value of 75 V. Finally, from Figure 7c,d, the third harmonic power-dependent proportional power distribution is validated, where each module delivers active power to the AC-side in proportion to the DC-side voltage of each module's k_N-factor. It is clearly seen from Figure 7c,d that the 611.2 W active power is delivered by each module MG2 and MG3, and the remaining required power of 277.8 W by SCMG is delivered by third harmonic power sharing, which clearly indicates that the proposed control in Figure 5 is working at its potential.

Table 1. Parameters for simulation analysis of SCMG.

Parameter	Value
Number of SCMG units	3
AC-side voltage (V_{rms})	220 V
AC-side rated power	1500 W
Case 1	
MG-1 rated capacitor voltage	75 V
MG-2 rated battery voltage	165 V
MG-3 rated battery voltage	165 V
Case 2	
MG-1 rated capacitor voltage	135 V
MG-2 rated battery voltage	135 V
MG-3 rated battery voltage	135 V
Case 3	
AC-side rated power	2000 W
SM battery rated capacity	30 Ah
Grid side inductance	5 mH
Carrier frequency	10 kHz

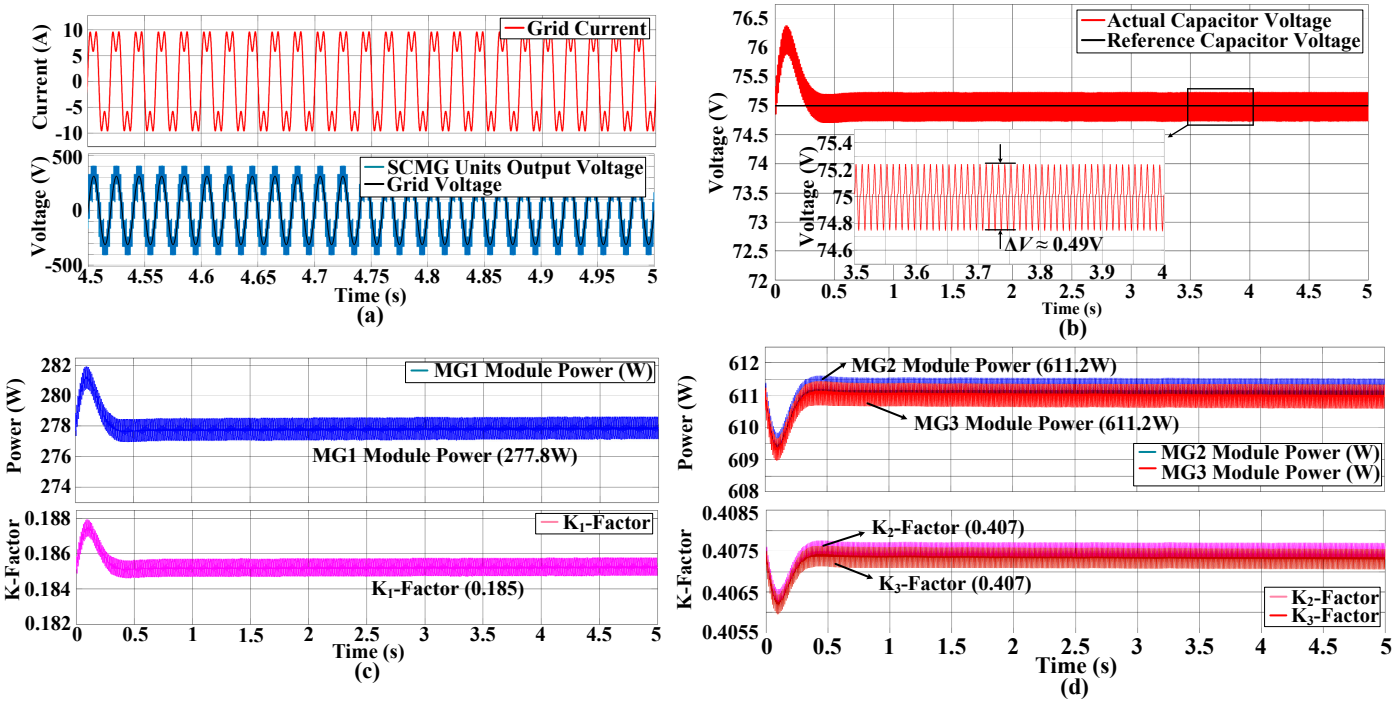

Figure 7. (**a**) Grid current (i_{g_pk} = 9.64 A) and SCMG modules output step-voltage (405 V) in-phase with grid voltage (v_{g_pk} = 311 V). (**b**) Capacitor voltage of MG1 balanced at 75 V. (**c**,**d**) Multi-power-carriers-based proportional power of MG1, MG2, and MG3, respectively, and corresponding K_N-factors.

Case #2: Power distribution when $V_{B1} + V_{B2} < v_{g\_pk}$

In this case, the SCMG is implemented where battery module voltage in MG2 is considered at V_{DC2} = 135 V and the battery module voltage in MG3 is considered at V_{DC3} = 135 V. As mentioned in Table 1, in this case, the capacitor voltage in MG3 should be balanced at V_{DC1} = 135 V and the seven-level SCMG units output voltage must be maintained at v_{MG} = 405 V over multi-power-carriers-based power distribution.

In Figure 8a, the seven-level output voltages in-phase with the grid voltage are maintained and remain stable over time during the capacitor voltage balancing in MG1 along with the stable grid current, which has the presence of injected third harmonic current. The results in Figure 8b clearly signify the capacitor voltage stability of MG1 at 135 V at 0.5 s, indicating the stable control of differential-mode power through injected third harmonic current. The multi-power-carriers-based third harmonic current-injected proportional power distribution is validated in Figure 8c, where each SCMG module delivers power in accordance with the k_N-factor, which is in proportion with the DC-side voltage of each module. The active power delivered by MG2 and MG3 is 500 W each, and the remaining required power of 500 W is compensated by third harmonic power sharing, which indicates that the proposed control (Figure 5) is working as anticipated.

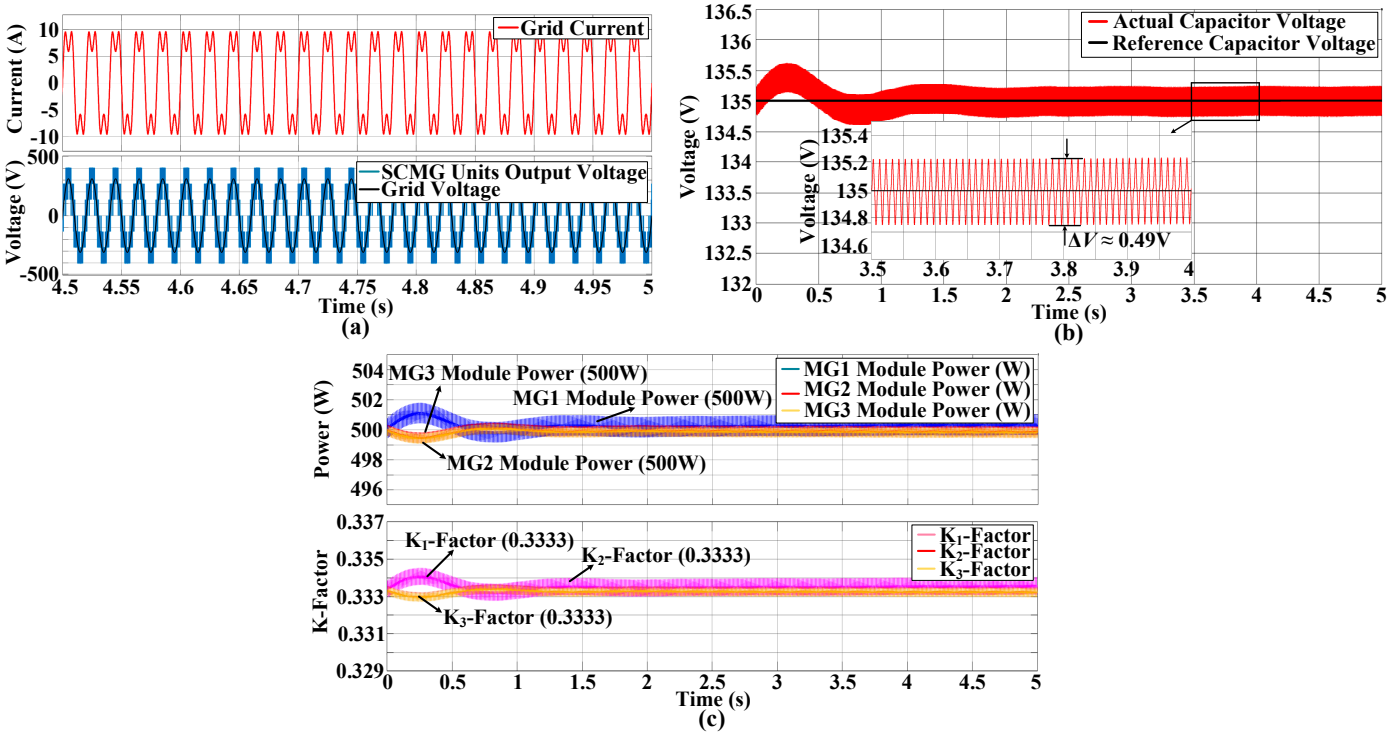

Figure 8. (**a**) Grid current (i_{g_pk} = 9.64 A) and SCMG modules output step-voltage (405 V) in-phase with grid voltage (v_{g_pk} = 311 V). (**b**) Capacitor voltage of MG1 balanced at 135 V. (**c**) Multi-power-carriers-based proportional power of MG1, MG2, and MG3, respectively, and corresponding K_N-factors.

Case #3: Abrupt Change in Grid Power Reference

The SCMG system is implemented in this scenario with the same parameters considered in *case 2*, as shown in Table 1. However, the grid power reference is abruptly changed at 2.5 s from 1500 W to 2000 W without increasing the grid voltage to examine the stability of the developed control. So, the grid current abruptly increased at 2.5 s to maintain to required active power demand. In this scenario, the SCMGs start to deliver more active power to the grid with the equivalent ratios of power-sharing with respect to their DC-side

voltages in order to meet the grid-side power demand while maintaining SCMGs output step-voltages.

Figure 9a represents the grid current (fundamental plus third harmonic current), which stabilized in a short time after a sudden increase in grid-side power demand at t = 2.5 s. It signifies that the developed integrated control (Figure 5) has the capability to work under various conditions. Figure 9b illustrates that the SCMG modules' output voltages were synchronized with the grid voltage while maintaining the seven-level step-voltages even during the change in power reference condition. Furthermore, the control maintains the stability of MG1's capacitor voltage in accordance with its reference voltage at 135 V again at 4.2 s, even after an abrupt change in grid-side power demand, see Figure 9c. Finally, Figure 9d confirms that each SCMG module delivers power proportional to its k_N-factor before and after the event of power variation. Before 2.5 s, MG2 delivered 500 W active power and MG3 delivered 500 W active power, and the remaining power demand of 500 W by SCMG was remunerated by third harmonic current injection; however, after 2.5 s, this remaining power demand increased to 666.67 W, which was still being compensated by our proposed control, as shown in Figure 5.

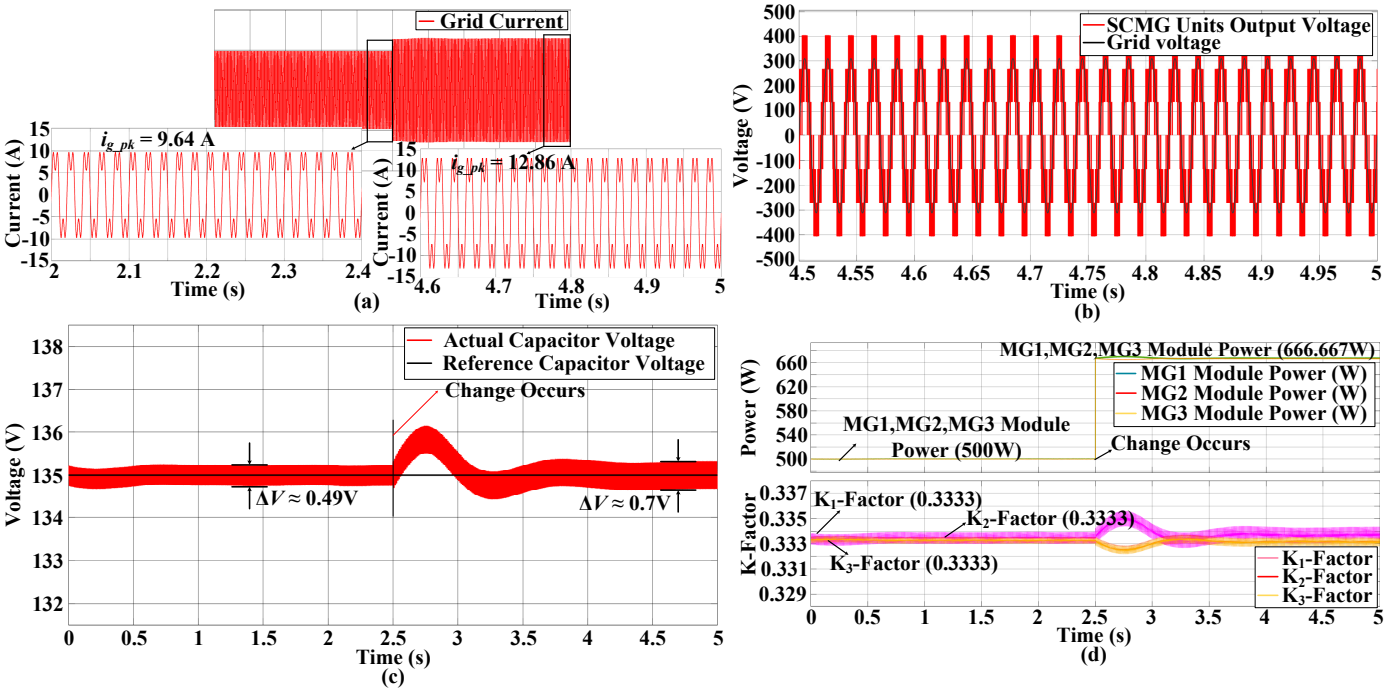

Figure 9. (**a**) Grid current (i_{g_pk} = 9.64 A) before abrupt change in grid power and grid current (i_{g_pk} = 12.84 A) after abrupt change in grid power. (**b**) Grid voltage (v_{g_pk} = 311 V) and SCMG modules output step-voltage (405 V). (**c**) Capacitor voltage of MG1 balanced at 135 V. (**d**) Multi-power-carriers-based proportional power of MG1, MG2, and MG3, respectively, and corresponding K_N-factors.

Finally, the hardware-in-loop platform (Typhoon HIL) was utilized for validation of developed control methodology (Figure 5) for power sharing in SCMG with the same parameters mentioned in Table 1 for simulation validation. Figure 10 shows the Typhoon HIL set-up for the real-time analysis used to further verify the Simulink analysis.

On the basis of the test set-up shown in Figure 10, Figure 11 presents the real-time results for the $V_{B1} + V_{B2} > v_{g\_pk}$ operating condition to verify case #1 examined in the simulation analysis; we realized that the MG1 capacitor voltage was stabilized at a reference value with the multi-power-carriers-based proportional power-sharing while seven-level SCMG output voltage was maintained along with the stable grid current.

Figure 10. Test set-up for real-time analysis.

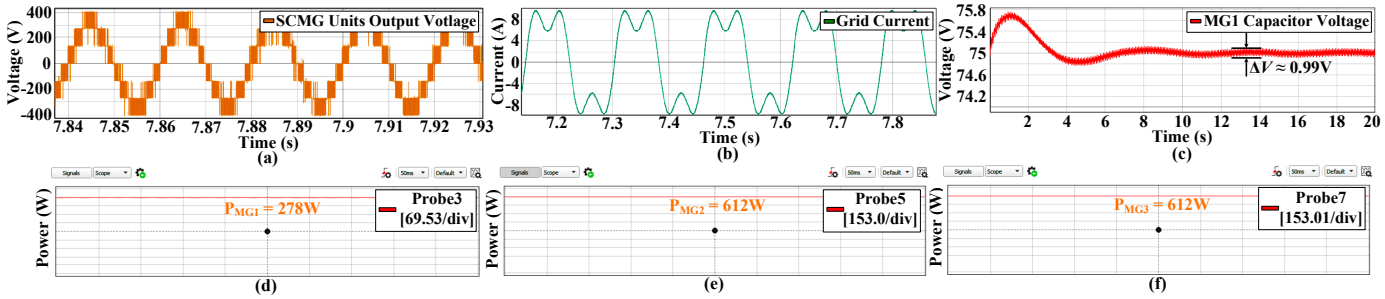

Figure 11. (**a**) SCMG modules output step-voltage (405 V) in real-time. (**b**) Grid current (i_{g_pk} = 9.64 A) in real-time. (**c**) Balanced capacitor voltage of MG1 balanced at 75 V in real-time. (**d**–**f**) Multi-power-carriers-based proportional power of MG1, MG2, and MG3, respectively.

Similarly, Figure 12 illustrates the real-time results through emulation set-up (Figure 10) to verify the operating condition of case #2 of the simulation analysis, where $V_{B1} + V_{B2} < v_{g\_pk}$. It was observed that under this condition, the voltage of MG1 capacitor achieved stabilization through optimal power sharing in the Typhoon HIL set-up as it attained in Simulink. Additionally, the output voltage of the seven-level SCMG remained stable, and the grid current was maintained at a steady level. The hardware-in-loop operation of the developed control methodology for SCMG's third harmonic current dependent power sharing, similar to Simulink, confirms the performance of control in the different operating conditions.

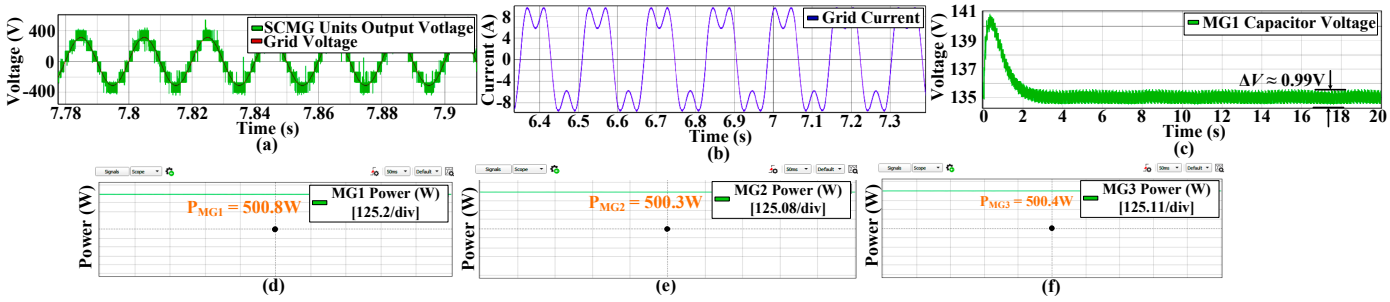

Figure 12. (**a**) SCMG modules output step-voltage (405 V) in real-time. (**b**) Grid current (i_{g_pk} = 9.64 A) in real-time. (**c**) Balanced capacitor voltage of MG1 balanced at 135 V in real-time. (**d**–**f**) Multi-power-carriers-based proportional power of MG1, MG2, and MG3.

Previous studies [7,9,18–20] have not examined the SCMG structure for worst-case conditions while also considering the PV module followed by a set of battery modules. In this proposed study, a multi-power-carriers-based integrated control is proposed in which the fundamental power is shared through fundamental current; however, for additional power demand, the third harmonic current injection coupled with the proportional power distribution method was developed. To justify this proposed control methodology, case studies were developed in which the battery modules were not only considered to be smoother but also capable of delivering the required voltage and power support to the

MG through third harmonic current injection while considering that the PV module power generation capacity is zero. In this methodology, the PV module's capacitor voltage was not only balanced via third harmonic power-sharing signal; additionally, it delivered the required power to the microgrid in the absence of PV module power. In case #2, the PV module power generation capability was zero and the battery modules power capacity was less than the power demanded by the microgrid; so, the remaining required power was delivered by the third harmonic current-injection methodology which signifies the extended power-sharing range of this proposed control.

5. Future Work

For the SCMG in grid-connected mode, the ring/delta-connection of SCMGs will be established on developed multi-carrier-based integrated control in future work. The power distribution in series-cascaded topologies is a valuable problem in worse-case scenarios, as is the one considered in this paper. So, this study will provide valuable insight to overcome the power distribution concern in series-cascaded topologies. Additionally, the limitation of the presence of a third harmonic current in the grid current will be resolved due to the fact that the injected third harmonic current will flow as a circulating current, which will aid in the power distribution control of ring-connected SCMG legs along with the power distribution between series-cascaded DG-based modules.

6. Conclusions

In this article, we presented an SCMG topology that integrates ND-DGs and battery energy storage-based modules. While working in different operating conditions, the SCMG structure has limited power-sharing capability in the existing literature; so, in this paper a control methodology with extended power-sharing range has been proposed. A multi-power-carriers-based integrated control was developed for optimal proportional power-sharing over a third harmonic power distribution signal in SCMG-DGs with the help of a third harmonic current injection in the fundamental frequency current of SCMG. The simulation and emulation analyses have demonstrated the effectiveness of the developed control methodology, in that the SC modules have achieved proportional power distribution in various scenarios with the help of k_N-factor. They have also demonstrated that the developed control has the capability to maintain the SCMG output step voltages while maintaining the module (MG1) capacitor voltages at a reference value and delivering the power support to the MG during zero irradiation levels of PV, which signifies the extended power distribution range of the developed control. Case #2 examined the maximum power-sharing range when the battery modules power capacity is less than the MG requirement and the PV module cannot deliver the remaining power due to it zero irradiation level. In this case, the remaining required power by the SCMG was delivered by the third harmonic power, which clearly signifies the extended power-sharing range of this proposed control. The practical application of the developed SCMG and its control encompasses the stable power distribution and flexible integration of ND-DGs and energy storage-based modules, particularly in environments with intermittent renewable energy. Depending on the performance of the developed methodology, the SCMG structure can be extended to include multiple ND-DGs along with the integration of D-DGs in a cascaded connection.

Author Contributions: Conceptualization, S.A., S.B.R. and M.M.K.; methodology, S.A., S.B.R. and M.M.K.; software, S.A.; validation, S.A., S.B.R. and M.M.K.; formal analysis, S.A. and M.M.K.; investigation, S.A.; resources, S.A. and S.B.R.; writing—original draft preparation, S.A.; writing—review and editing, S.A., S.B.R., M.M.K. and F.C.; visualization, S.A.; supervision, S.B.R., M.M.K. and F.C.; project administration, S.B.R. and F.C.; funding acquisition, S.B.R. and F.C. All authors have read and agreed to the published version of the manuscript.

Funding: This work was supported by the Ministerio de Ciencia e Innovación under Grant PID2021-123633OB-C33.

Data Availability Statement: Data are contained within the article.

Acknowledgments: We thank the reviewers for their useful comments and suggestion.

Conflicts of Interest: The authors declare no conflicts of interest.

References

1. Sun, Y.; Hou, X.; Yang, J.; Han, H.; Su, M.; Guerrero, J.M. New Perspectives on Droop Control in AC Microgrid. *IEEE Trans. Ind. Electron.* **2017**, *64*, 5741–5745. [CrossRef]
2. Nutkani, I.U.; Loh, P.C.; Wang, P.; Blaabjerg, F. Cost-Prioritized Droop Schemes for Autonomous AC Microgrids. *IEEE Trans. Power Electron.* **2015**, *30*, 1109–1119. [CrossRef]
3. Lu, F.; Choi, B.; Maksimovic, D. Autonomous Power-Source Regulation in Series-Connected Low-Voltage Microinverters. *IEEE J. Emerg. Sel. Top. Power Electron.* **2020**, *8*, 1442–1453. [CrossRef]
4. Ali, S.; Ling, Z.; Tian, K.; Huang, Z. Recent Advancements in Submodule Topologies and Applications of MMC. *IEEE J. Emerg. Sel. Top. Power Electron.* **2020**, *9*, 3407–3435. [CrossRef]
5. Kjaer, S.B.; Pedersen, J.K.; Blaabjerg, F. A Review of Single-Phase Grid-Connected Inverters for Photovoltaic Modules. *IEEE Trans. Ind. Appl.* **2005**, *41*, 1292–1306. [CrossRef]
6. Maharjan, L.; Inoue, S.; Akagi, H.; Asakura, J. State-of-Charge (SOC)-Balancing Control of a Battery Energy Storage System Based on a Cascade PWM Converter. *IEEE Trans. Power Electron.* **2009**, *24*, 1628–1636. [CrossRef]
7. He, J.; Li, Y.; Liang, B.; Wang, C. Inverse Power Factor Droop Control for Decentralized Power Sharing in Series-Connected-Microconverters-Based Islanding Microgrids. *IEEE Trans. Ind. Electron.* **2017**, *64*, 7444–7454. [CrossRef]
8. Tian, K.; Ali, S.; Huang, Z.; Ling, Z. Power Control and Experiment of 2MW/10kV Cascaded H-Bridge Power Conversion System for Battery Energy Storage System. In Proceedings of the 8th Renewable Power Generation Conference (RPG 2019), Shanghai, China, 24–25 October 2019; pp. 1–7.
9. Sun, Y.; Shi, G.; Li, X.; Yuan, W.; Su, M.; Han, H.; Hou, X. An F-P/Q Droop Control in Cascaded-Type Microgrid. *IEEE Trans. Power Syst.* **2018**, *33*, 1136–1138. [CrossRef]
10. Ali, S.; Bogarra, S.; Khan, M.M.; Taha, A.; Phyo, P.P.; Byun, Y.-C. Prospective Submodule Topologies for MMC-BESS and Its Control Analysis with HBSM. *Electronics* **2023**, *12*, 20. [CrossRef]
11. Walker, G.R.; Sernia, P.C. Cascaded DC-DC Converter Connection of Photovoltaic Modules. *IEEE Trans. Power Electron.* **2004**, *19*, 1130–1139. [CrossRef]
12. Villanueva, E.; Correa, P.; Rodriguez, J.; Pacas, M. Control of a Single-Phase Cascaded H-Bridge Multilevel Inverter for Grid-Connected Photovoltaic Systems. *IEEE Trans. Ind. Electron.* **2009**, *56*, 4399–4406. [CrossRef]
13. Yuan, W.; Wang, Y.; Ge, X.; Hou, X.; Han, H. A Unified Distributed Control Strategy for Hybrid Cascaded-Parallel Microgrid. *IEEE Trans. Energy Convers.* **2019**, *34*, 2029–2040. [CrossRef]
14. He, J.; Liu, X.; Mu, C.; Wang, C. Hierarchical Control of Series-Connected String Converter-Based Islanded Electrical Power System. *IEEE Trans. Power Electron.* **2020**, *35*, 359–372. [CrossRef]
15. He, J.; Liu, Y.; Wang, Y. Cascaded Droop and Inverse Droop Regulation for Two-Layer Coordinated Power Flow Control in Series-Connected Power Cells. *IEEE Trans. Ind. Electron.* **2021**, *68*, 6939–6951. [CrossRef]
16. He, J.; Li, Y.; Wang, C.; Pan, Y.; Zhang, C.; Xing, X. Hybrid Microgrid With Parallel- and Series-Connected Microconverters. *IEEE Trans. Power Electron.* **2018**, *33*, 4817–4831. [CrossRef]
17. Li, L.; Sun, Y.; Han, H.; Shi, G.; Su, M.; Zheng, M. A Decentralized Control for Cascaded Inverters in Grid-Connected Applications. *IEEE Trans. Ind. Electron.* **2020**, *67*, 8064–8071. [CrossRef]
18. Li, L.; Ye, H.; Liu, Z.; Han, H.; Sun, Y.; Su, M. Decentralized Economical-Sharing Scheme for Cascaded AC Microgrids. In Proceedings of the 2017 IEEE Energy Conversion Congress and Exposition (ECCE), Cincinnati, OH, USA, 1–5 October 2017; pp. 3736–3740.
19. Das, S.; Nutkani, I.U.; Teixeira, C. Decentralised Master-Slave Control for Series-Cascaded AC Microgrid Integrating Solar Photovoltaic Generation. In Proceedings of the 2019 IEEE International Conference on Industrial Technology (ICIT), Melbourne, Australia, 13–15 February 2019; pp. 417–422.
20. Das, S.; Nutkani, I.U.; Teixeira, C.A. Decentralized Master–Slave Control for Series-Cascaded Islanded AC Microgrid. *IEEE Trans. Ind. Electron.* **2022**, *69*, 5942–5951. [CrossRef]
21. Li, L.; Sun, Y.; Su, M.; Fu, S. Decentralized Mutual Damping Control of Cascaded-Type VSGs for Power and Frequency Oscillation Suppression. *IEEE Trans. Ind. Electron.* **2022**, *69*, 10215–10226. [CrossRef]
22. Amamra, S.; Meghriche, K.; Cherifi, A.; Francois, B. Multilevel Inverter Topology for Renewable Energy Grid Integration. *IEEE Trans. Ind. Electron.* **2017**, *64*, 8855–8866. [CrossRef]
23. Zhang, Q. Control of PV Battery Hybrid System Using Cascaded H Bridge Converter. In Proceedings of the 2017 IEEE 3rd International Future Energy Electronics Conference and ECCE Asia (IFEEC 2017—ECCE Asia), Kaohsiung, Taiwan, 3–7 June 2017; pp. 2008–2012.
24. Huang, Q.; Wang, M.; Yu, W.; Huang, A.Q. Power-Weighting-Based Multiple Input and Multiple Output Control Strategy for Single-Phase PV Cascaded H-Bridge Multilevel Grid-Connected Inverter. In Proceedings of the 2015 IEEE Applied Power Electronics Conference and Exposition (APEC), Charlotte, NC, USA, 15–19 March 2015; pp. 2148–2153.

25. Chavarria, J.; Biel, D.; Guinjoan, F.; Meza, C.; Negroni, J.J. Energy-Balance Control of PV Cascaded Multilevel Grid-Connected Inverters Under Level-Shifted and Phase-Shifted PWMs. *IEEE Trans. Ind. Electron.* **2013**, *60*, 98–111. [CrossRef]
26. Zhao, T.; Wang, G.; Bhattacharya, S.; Huang, A.Q. Voltage and Power Balance Control for a Cascaded H-Bridge Converter-Based Solid-State Transformer. *IEEE Trans. Power Electron.* **2013**, *28*, 1523–1532. [CrossRef]
27. Ko, Y.; Andresen, M.; Buticchi, G.; Liserre, M. Power Routing for Cascaded H-Bridge Converters. *IEEE Trans. Power Electron.* **2017**, *32*, 9435–9446. [CrossRef]
28. Zhao, T.; Zhang, X.; Mao, W.; Wang, F.; Xu, J.; Gu, Y.; Wang, X. An Optimized Third Harmonic Compensation Strategy for Single-Phase Cascaded H-Bridge Photovoltaic Inverter. *IEEE Trans. Ind. Electron.* **2018**, *65*, 8635–8645. [CrossRef]
29. Nutkani, I.U.; Teixeira, C.; Acuna, P.; Mcgrath, B. Series-Cascaded AC Microgrid Topology Integrating Non-Dispatchable Distributed Generation and Storage. In Proceedings of the 2018 IEEE 27th International Symposium on Industrial Electronics (ISIE), Cairns, Australia, 13–15 June 2018; pp. 67–73.
30. Zhang, L.; Sun, K.; Huang, Z.; Li, Y.W. A Grid-Tied Photovoltaic Generation System Based on Series-Connected Module Integrated Inverters with Adjustable Power Factor. In Proceedings of the 2015 IEEE Energy Conversion Congress and Exposition (ECCE), Montreal, QC, Canada, 20–24 September 2015; pp. 6864–6870.
31. Lu, F.; Choi, B.; Maksimovic, D. Autonomous Control of Series-Connected Low Voltage Photovoltaic Microinverters. In Proceedings of the 2015 IEEE 16th Workshop on Control and Modeling for Power Electronics (COMPEL), Vancouver, BC, Canada, 12–15 July 2015; pp. 1–6.